Analysis of intercore crosstalk of WDM channels around zero-dispersion wavelength in homogeneous multicore fibers

Monica López-Coyote,[a] **Daniel E. Ceballos-Herrera**,[a,*] **Ramón Gutiérrez-Castrejón**,[a] **Herman L. Offerhauss**,[b] **and José A. Álvarez-Chávez**[b]

[a]Universidad Nacional Autónoma de México, Instituto de Ingeniería, Coyoacán, México
[b]University of Twente, Optical Sciences Group, Enschede, The Netherlands

Abstract. We present a numerical analysis of the average intercore crosstalk (IC-XT) of wavelength-division multiplexed (WDM) optical channels in a homogeneous two-core fiber system. This analysis is performed considering cores with zero-dispersion wavelengths at 1550 nm. In the analysis, we consider 11 WDM channels spaced 100 GHz apart transmitted in three different schemes, one centered at 1510 nm with negative dispersion $D = -3.5$ ps/nm · km, one centered at 1550 nm with $D = 0$, and one centered at 1590 nm with $D = +3.5$ ps/nm · km. This selection allows for the observation of how the IC-XT of WDM channels is modified using positive, zero, and negative dispersion parameters. To analyze more realistic scenarios of IC-XT in multicore fibers, we considered random bending and twisting perturbations along the fiber. In addition, we considered fiber nonlinearities such as four-wave mixing (FWM) among WDM channels. The results show that FWM produces a power transfer among the transmitted WDM channels that depends on the dispersion parameter D at core 1, and this effect is transferred to the average crosstalk of the WDM channels at core 2. Therefore, the average IC-XT of WDM channels can be modified in a controlled way by selecting an adequate dispersion parameter D in combination with FWM nonlinearity. These results provide valuable information for understanding the wavelength dependence of the average IC-XT of homogeneous multichannel MCF systems working around a zero-dispersion wavelength. [DOI: 10.1117/1.OE.60.7.076107]

Keywords: multicore fiber; intercore crosstalk; WDM channels; zero-dispersion wavelength.

Paper 20210302 received Mar. 18, 2021; accepted for publication Jul. 9, 2021; published online Jul. 21, 2021.

1 Introduction

Spatial division multiplexing (SDM) based on multicore fibers (MCFs) has been recently investigated as a key element of increasing the capacity of future fiber transmission systems. In MCFs, the signals that propagate in each core can be coupled to another core by linear and nonlinear coupling mechanisms, producing intercore crosstalk (IC-XT) that induces power degradation of the propagated data signals in each core. As a consequence, IC-XT must be reduced as much as possible to improve the performance of SDM systems.[1–4] In addition, this IC-XT randomly changes along the MCF due to random structural and external perturbations. Therefore, it is important to consider the statistical average of the IC-XT. Recently, a theoretical expression for the average IC-XT has been deduced, which is valid only for a weak coupling regime in which MCFs with a core separation higher than 30 μm are considered.[1,2]

On the other hand, to achieve ultrahigh capacity transmission in MCFs, it is mandatory to consider multiple wavelength-division multiplexed (WDM) optical channels across the C and L bands in each core. In this context, extensive studies have been performed to determine the IC-XT of each WDM channel in MCFs.[5] This information would allow us to select the most

*Address all correspondence to Daniel E. Ceballos-Herrera, DCeballosH@iingen.unam.mx

0091-3286/2021/$28.00

convenient modulation formats and forward error correction schemes (FECs) for different groups of WDM channels that propagate in each core. The first study on this matter was performed in MCFs with perfectly homogeneous cores under a weak coupling regime. It was shown that the wavelength dependence of the average IC-XT is governed by the coupling coefficient, which increases linearly with wavelength.[5] As a consequence, the IC-XT of each WDM channel also increases for longer wavelengths. More advanced studies have been performed to understand in detail the IC-XT of WDM channels in homogeneous MCFs by including the combined effect of the most common nonlinearities found in WDM-transmission systems: cross-phase modulation (XPM), four-wave mixing (FWM), and stimulated Raman scattering (SRS).[6–8] As a result, it was found that the power transfer among the transmitted WDM channels caused by SRS and FWM nonlinearities can modify the average IC-XT in a comparable magnitude to this produced by only considering the wavelength dependence of the linear coupling coefficient.[6–8] Therefore, linear and nonlinear effects can be combined in a controlled way to modify the average IC-XT of WDM channels.

In this context, in all of these studies, only homogeneous MCFs with a positive dispersion parameter (D) in their cores have been considered. The typical values of the dispersion parameter employed in each core is $D = 16$ ps/nm · km at 1550 nm, which corresponds to standard step-index single-mode-fiber cores in the MCF design.[7–10] In this sense, the impact of the dispersion parameter on the average IC-XT of multiple WDM optical channels is still to be assessed, mainly in MCFs that present negative and zero dispersion parameters at 1550 nm, such as MCFs with a trench-assisted refractive-index profile in their cores.[11,12] Therefore, due to the diversity of MCFs designs that employ different dispersion parameters, it is convenient to analyze how the power transfer among WDM channels caused by nonlinearities in cores with negative, zero, or positive dispersion could affect the IC-XT of wideband WDM channels in MCF systems. In this context, we numerically investigate the transmission of 11 WDM channels with a spectral position that is centered and shifted around a zero-dispersion wavelength in a homogeneous two-core fiber system with the goal of analyzing the dispersion impact on the wavelength dependence of the average IC-XT of WDM channels. This analysis is performed using theoretical formalism based on coupled propagation equations that includes fiber nonlinearities in the presence of random perturbations. We demonstrate that the dispersion parameter D of the MCF significantly affects the power transfer among WDM channels produced by FWM at core 1, modifying in consequence the average IC-XT of WDM optical channels at core 2. Then, the average IC-XT of WDM channels can be modified by selecting a specific dispersion parameter D of the MCF in combination with fiber nonlinearities. These results provide valuable information for understanding the wavelength dependence of the average IC-XT of WDM channels in homogeneous MCF systems working around a zero-dispersion wavelength or dispersion management systems that could be based on multiple MCF sections with positive and negative dispersion parameters.

2 Multicore Propagation Model

Let us first consider the total complex electric field of a pulse with spectrum centered at ω_0 in a heterogeneous single-mode multicore optical fiber with N cores:

$$\tilde{E} = \sum_{p}^{N} F_p(x,y)\tilde{A}_p(z,\omega-\omega_0)e^{i\beta_p(\omega_0)z} \Big/ \sqrt{N_p}, \tag{1}$$

where $\tilde{A}_p$ and $F_p(x,y)$ are the slowly varying amplitude of the pulse and the spatial distribution of the fundamental mode at core p and $\beta_p(\omega_0) = \beta_{0,p}$ is the propagation constant at the carrier frecuency ω_0. The expression in Eq. (1) is valid if the bandwidth $\Delta\omega$ of the pulse spectrum obeys the condition $\Delta\omega/\omega_0 \ll 1$, which implies pulses as short as 0.1 ps.[13] The power carried by the fundamental mode is expressed as $N_p = \frac{1}{2}\varepsilon_0 n_{\mathrm{eff},p} c I_p$, where $I_p = \iint F_p(x,y)^2 \mathrm{d}x\,\mathrm{d}y$, ε_0 is the vacuum permittivity, $n_{\mathrm{eff},p}$ is the effective refractive index of the fundamental mode at core p, and c stands for the speed of light. For simplicity, we consider that each core mode is linearly polarized and assume that all WDM channels are copolarized, which corresponds to the

worst-case scenario for FWM-induced power transfer in WDM systems. Therefore, the pulse propagation equation for the pulse envelope A_p at core p is given by[7]

$$\frac{\partial A_p}{\partial z} = \left(-\beta_{1,p}\frac{d}{dt} - i\frac{\beta_{2,p}}{2}\frac{d^2}{dt^2} + \frac{\beta_{3,p}}{6}\frac{d^3}{dt^3} + \ldots\right)A_p - \frac{\alpha}{2}A_p + i\sum_{l=1}^{N}\left\{\left(\frac{n_{\mathrm{eff},p}}{n_{\mathrm{eff},l}}\right)^{1/2} q_{p,l}A_l e^{-i\Delta\beta_{p,l}z}\right\} + i\sum_{l,m,n=1}^{N}\left\{\gamma_p f_{plmn}\left[\frac{(n_{\mathrm{eff},p})^{3/2}}{(n_{\mathrm{eff},l})^{1/2}(n_{\mathrm{eff},m})^{1/2}(n_{\mathrm{eff},n})^{1/2}}\right] \cdot \left[A_l e^{-i(\Delta\beta_{p,l}+\Delta\beta_{m,n})z}\int_{-\infty}^{t} R(t-t')A_m(t')A_n^*(t')\mathrm{d}t'\right]\right\}, \tag{2}$$

where p, l, m, n can take on values: 1,2, ..N and A_l, A_m, and A_n are the pulse envelopes of different cores. $\beta_{1,p}, \beta_{2,p}, \beta_{3,p}$ are the inverse of the group velocity, the group velocity dispersion (GVD), and the third-order dispersion at ω_0 of the fundamental mode in core p, respectively, $\Delta\beta_{p,l} = \beta_{0,p} - \beta_{0,l}$ and $\Delta\beta_{m,n} = \beta_{0,m} - \beta_{0,n}$ are the differences on the propagation constants between cores, and $\alpha = 0.2$ dB/km is the fiber loss coefficient. The term $R(t) = (1 - f_R)\delta(t) + f_R h_R(t)$ is the nonlinear response that includes both instantaneous electronic and delayed Raman contributions with $f_R = 0.18$. The function $h_R(t)$ for silica fibers is obtained using the analytical expression described in Ref. 14. Note that this expression simultaneously models all NL effects due to self-phase modulation and XPM, FWM, and SRS. The nonlinear coefficient is $\gamma_p = 3k_0\chi^{(3)}/(4\varepsilon_0 {n_{\mathrm{eff},p}}^2 c A_{\mathrm{eff},p})$, with $A_{\mathrm{eff},p}$ being the effective mode area at core p. Finally, the linear and nonlinear coupling coefficients are given as[3,7]

$$q_{p,l} = \left(\frac{k_0^2}{2\beta_{0,p}\sqrt{I_p}\sqrt{I_l}}\right)\iint F_p(x,y)^*\Delta n_p^2 F_l(x,y)\mathrm{d}x\,\mathrm{d}y, \tag{3}$$

$$f_{plmn} = \left(\frac{A_{\mathrm{eff},p}}{\sqrt{I_l}\sqrt{I_m}\sqrt{I_n}\sqrt{I_p}}\right)\iint F_l F_m F_n F_p \mathrm{d}x\,\mathrm{d}y, \tag{4}$$

where $k_0 = 2\pi/\lambda$, $\Delta n_p^2 = n^2 - n_p^2$, $n = n(x,y)$ is the spatial distribution of the multicore refractive index, and $n_p = n_p(x,y)$ is the refractive index of core p. These expressions follow the same nomenclature as in Refs. 3, 7, and 13 for a scalar nonlinear pulse propagation equation.

For the case of a two-core fiber with $N = 2$, we have the following linear and nonlinear coupling coefficients for core 1 ($p = 1$): q_{11}, q_{12}, f_{1111}, f_{1222}, $f_{1112} = f_{1121} = f_{1211}$, $f_{1122} = f_{1212} = f_{1221}$ and for core 2 ($p = 2$): q_{22}, q_{21}, f_{2222}, f_{2111}, $f_{2221} = f_{2212} = f_{2122}$, $f_{2211} = f_{2121} = f_{2112}$ respectively. In addition, for MCFs under a weak coupling regimen with a core separation higher than 30 μm, the nonlinear intercore coupling coefficients f_{1222}, f_{1112}, f_{1122}, f_{2111}, f_{2221}, f_{2211} are several orders of magnitude smaller than the intracore coupling coefficients f_{1111}, f_{2222}; as a consequence, only intracore nonlinear coefficients f_{1111}, f_{2222} are considered in the coupled propagation equations.[3,7,8] Therefore, the coupled equations for a two-core fiber system under a weak coupling regime are approximated as follows:

$$\frac{\partial A_p}{\partial z} = \left(-\beta_{1,p}\frac{d}{dt} - i\frac{\beta_{2,p}}{2}\frac{d^2}{dt^2} + \frac{\beta_{3,p}}{6}\frac{d^3}{dt^3} + \ldots\right)A_p - \frac{\alpha}{2}A_p + i\sum_{l=1}^{N}\left\{\left(\frac{n_{\mathrm{eff},\ p}}{n_{\mathrm{eff},l}}\right)^{1/2} q_{p,l}A_l e^{-i\Delta\beta_{p,l}z}\right\} + i\gamma_p\, f_{pppp}\cdot\left[A_p\int_{-\infty}^{t} R(t-t')|A_p(t')|^2\mathrm{d}t'\right]\Bigg\} \tag{5}$$

where $p, l = 1,2$ correspond to each fiber core.

On the other hand, to introduce external perturbations induced by bending and twisting in the signal phase of each core, we rewrite the exponential terms in Eq. (5) as $e^{-i\Delta\beta_{p,l}z} = e^{-i\Delta\phi_{p,l}(z)}$. The perturbed phase mismatch $\Delta\phi_{p,l}(z)$ is given as[2]

$$\Delta\phi_{p,l}(z) = (\beta_{0,p} - \beta_{0,l})z - \beta_{0,l}\int_0^z \frac{d}{R}\cos(f\tau + \theta_l)\mathrm{d}\tau, \tag{6}$$

where R is the bending radius, d is the core pitch between p and l cores, f is the twist rate, and θ_l is the offset of the twist angle of core l at $z = 0$[2]. In our analysis, for simplicity we assumed $\theta_l = 0$. In addition, for homogeneous cores, we have $n_{\mathrm{eff},p} = n_{\mathrm{eff},l}$ and $\beta_{0,p} - \beta_{0,l} = 0$; then, according to Eq. (6), the phase mismatch is caused only by twists and bending. Also, for the case of two cores ($p = 1, 2$), the IC-XT from core 1 to core 2 is calculated as follows: $XT = |A_2(z)|^2/|A_1(z)|^2$. In addition, if we consider random variations of R and f along the fiber in Eq. (6), it modifies the solutions $A_1(z)$ and $A_2(z)$ given by Eq. (5), and we can generate a random IC-XT from core 1 to core 2 for each WDM channel.

3 Numerical Model and Results

To investigate the transmission of multiple WDM optical channels in the two-core fiber system, Eq. (5) has been numerically solved using the split-step Fourier method for 11 WDM channels spaced 100 GHz apart, leading to a total WDM bandwidth of 1 THz (~8 nm). The numerical setup employed in our simulations is shown in Fig. 1. In addition, 1024-bit long sequences consisting of Gaussian pulses having a 20-ps pulse-width and running at 10 Gb/s were employed in each optical WDM channel. The input average power of each WDM signal was set to 5 mW in core 1 and 0 mW in core 2. For the analysis of fiber nonlinear effects, higher signal power values per WDM channel were utilized.

The cores considered in our simulation have a zero-dispersion wavelength at 1550 nm. The refractive index profile of each core is shown in Fig. 2. The Sellmeier equation of SiO_2 employed to obtain the refractive index profile at different wavelengths is defined in Eq. (2) of Ref. 15 with a mole fraction of 0.09796% GeO_2 for n_1, a mole fraction of 0.021% GeO_2 for n_2, and 0% of GeO_2 for n_3, respectively.

To analyze a weak coupling regime between core 1 and core 2, we considered a core separation of $d = 33.7$ μm similar to Refs. 1, 10–12. A simulated view of the fundamental modes $F_p(x, y)$ in each core can be seen in Fig. 3 for 1550 nm, which were obtained by simulation based on a fast Fourier transform mode solver.[16] The effective area and nonlinear coefficient calculated for each core are $A_{\mathrm{eff}} = 53.43$ $\mu\mathrm{m}^2$ and $\gamma_p = 2.14$ $\mathrm{W}^{-1}\,\mathrm{km}^{-1}$. The linear coupling coefficients calculated at 1550 nm are $q_{1,1} = q_{2,2} = 3.4 \times 10^{-5}$ m^{-1} and $q_{1,2} = q_{2,1} = 0.1$ m^{-1}. These coupling coefficients were obtained using Eq. (3) and considering the refractive index profile given in Fig. 2 and the modal fields given in Fig. 3, respectively.

To analyze the IC-XT of multiple WDM channels, we calculated the coupling coefficients at different wavelengths. Using polynomial regression, we obtained the following relations: $q_{11} = 0.4204 - 0.0011\lambda + 1.2114 \times 10^{-6}\lambda^2 - 5.6021 \times 10^{-10}\lambda^3 + 9.7217 \times 10^{-14}\lambda^4$, and

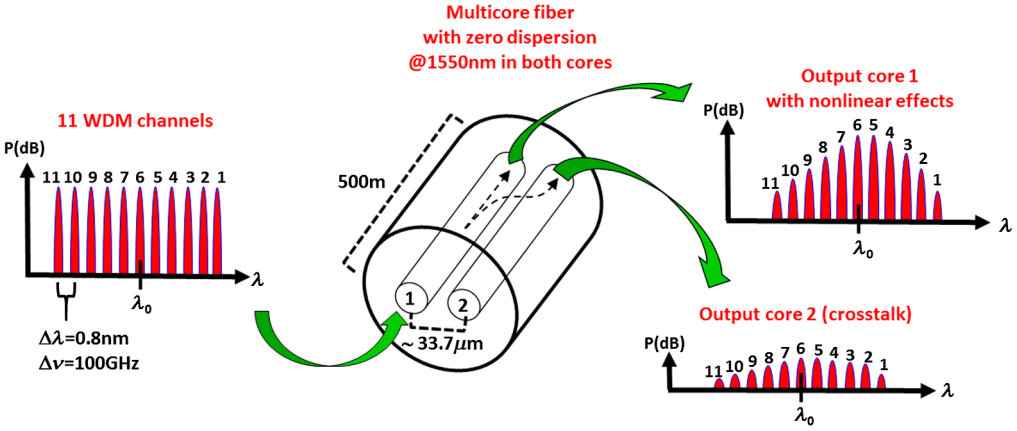

Fig. 1 Numerical setup.

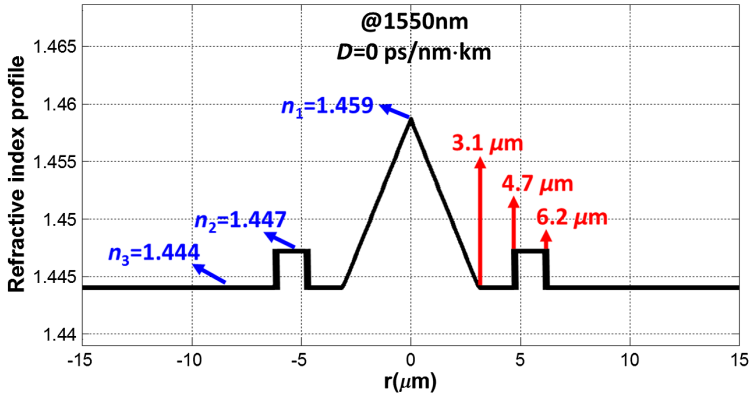

Fig. 2 Refractive index profile of each core at 1550 nm. The blue arrows indicate the refractive index values of the different layers in the fiber core, and the red arrows indicate the radius of each layer in the fiber core.

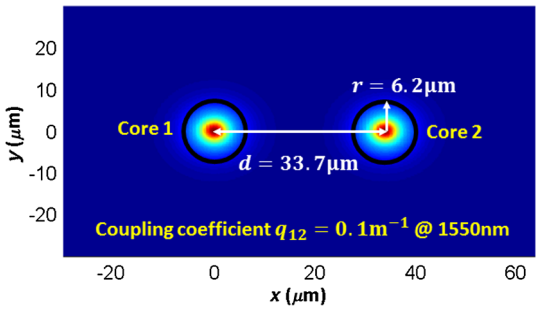

Fig. 3 Simulated view of the core modes at 1550 nm. The black circle indicates the fiber core perimeter.

$q_{12} = 48.6904 - 0.1450\lambda + 1.6285 \times 10^{-4}\lambda^2 - 8.1672 \times 10^{-8}\lambda^3 + 1.5443 \times 10^{-11}\lambda^4$, where q_{11} and q_{12} are in (1/m) and λ is in (nm).

On the other hand, we considered three different WDM transmission schemes: one centered at 1510 nm with negative dispersion parameter $D = -3.4$ ps/nm · km, one centered at 1550 nm with zero dispersion parameter $D = 0$, and one centered at 1590 nm with positive dispersion parameter $D = +3.4$ ps/nm · km, respectively. These WDM transmission schemes are described in Fig. 4, where we can observe how each WDM scheme is placed on the dispersion curve of the MCF.

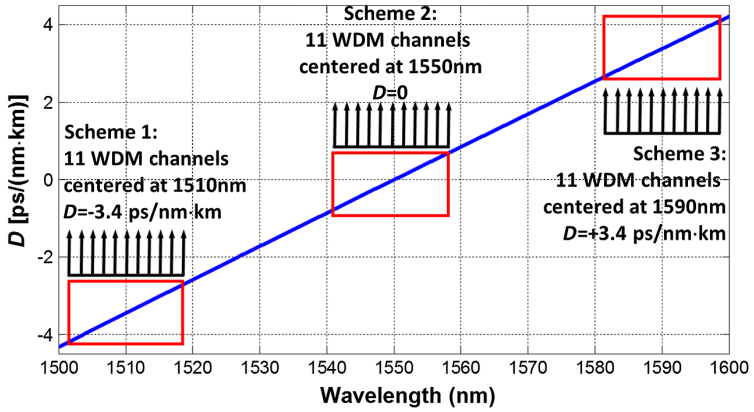

Fig. 4 WDM schemes employed at the input of core 1 in the MCF.

For the WDM scheme 1 centered at $\lambda_0 = 1510$ nm, we employed the following dispersion coefficients: $\beta_{0,p} = 6.0205 \times 10^9$ km^{-1}, $\beta_{1,p} = 4.8980 \times 10^6$ ps/km, $\beta_{2,p} = 4.1517$ ps^2/km, and $\beta_{3,p} = 0.1205$ ps^3/km. These values are employed in Eq. (5) and allow for a dispersion parameter $D = -\frac{2\pi c}{\lambda_0^2}\beta_{2,p} = -3.4$ ps/nm · km. On the other hand, for the WDM scheme 2 centered at $\lambda_0 = 1550$ nm, we used $\beta_{0,p} = 5.8627 \times 10^9$ km^{-1}, $\beta_{1,p} = 4.8979 \times 10^6$ ps/km, $\beta_{2,p} = 0$, and $\beta_{3,p} = 0.1387$ ps^3/km, which allow for a dispersion parameter $D = 0$ ps/nm · km. Finally, for the WDM scheme 3 centered at $\lambda_0 = 1590$ nm, we used the coefficients $\beta_{0,p} = 5.7128 \times 10^9$ km^{-1}, $\beta_{1,p} = 4.8980 \times 10^6$ ps/km, $\beta_{2,p} = -4.5644$ ps^2/km, and $\beta_{3,p} = 0.1581$ ps^3/km, which allow for a dispersion parameter $D = -\frac{2\pi c}{\lambda_0^2}\beta_{2,p} = +3.4$ ps/nm · km, respectively.

As is indicated in Fig. 1, the input of core 1 is composed of 11 WDM channels while the input of core 2 is zero. In this way, we can analyze the IC-XT of each WDM channel from core 1 to core 2. To perform the modeling of IC-XT, the two-core fiber length was set to $L = 500$ m to achieve acceptable IC-XT power levels while ensuring moderate computation times similar to Refs. 8 and 9. In addition, we have divided the fiber into a large number of segments that are 0.25 m long each, which correspond to the phase matching points.[2,8,9] Both R and f remain constant in each segment but change randomly from segment to segment according to the absolute value of Gaussian distributions with mean values given by $\langle R \rangle = 0.2$ m and $\langle f \rangle = 4\pi$ rad/m, with standard deviations of 30% to evaluate scenarios in which the MCF is spooled on a reel. We also introduced a moving average method to obtain smooth transitions of R and f along the fiber. The Δz step employed in our simulations was 0.1 mm. Finally, we carried out 1000 runs to obtain an average IC-XT from core 1 to core 2. We also calculated the theoretical average crosstalk of two adjacent cores in a homogenous MCF given in Eq. (27) of Ref. 2: $XT_\mu = 2{q_{1.2}}^2 \cdot \langle R \rangle \cdot L/[\beta_{0,1} \cdot d]$. In particular, this theoretical expression is valid only for pulse propagation without fiber nonlinearities, Then, as a first step, we perform the simulations and calculate the theoretical average IC-XT considering a nonlinear coefficient zero ($\gamma_p = 0$). As a result, we obtain the plots shown in Fig. 5, which correspond to the average IC-XT of 11 WDM channels for three WDM transmission schemes centered at 1510, 1550, and 1590 nm, respectively. As is shown in Fig. 5, a comparison of our simulations with the theoretical approach led to very good agreement taking into account that this expression is only valid for linear coupling

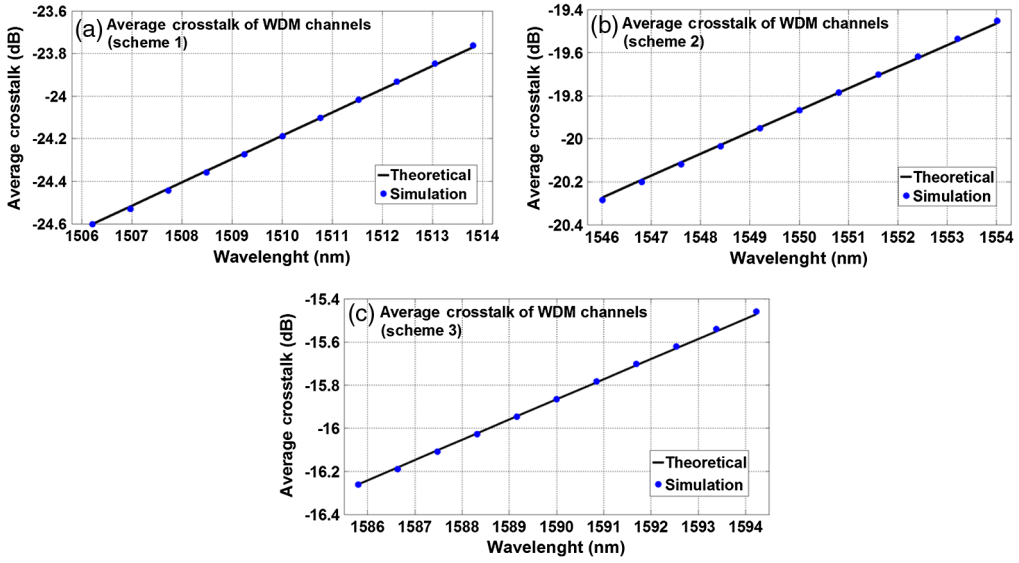

Fig. 5 Average IC-XT of 11 WDM channels at core 2 as function of wavelength for three WDM transmission schemes centered at (a) 1510 nm, (b) 1550 nm, and (c) 1590 nm. A black solid curve that corresponds to the theoretical average crosstalk superposes the blue points obtained by numerical simulation. The fiber length is 500 m.

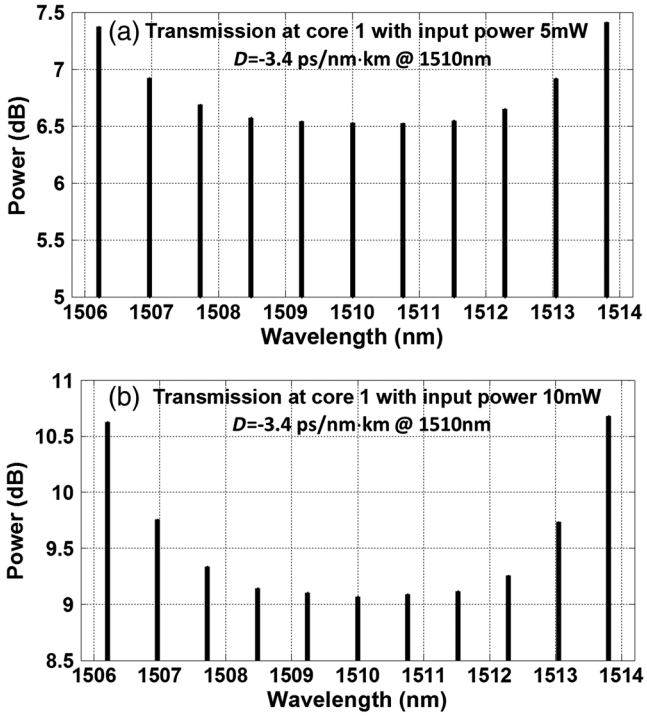

Fig. 6 Transmission of 11 WDM channels centered at 1510 nm in core 1 for a propagation length of 500 m with (a) 5 mW (6.99 dB) and (b) 10 mW (10 dB) of input power per WDM channel.

scenarios like ours with $q_{pl} \gg f_{plmn}$. From Fig. 5, the linear behavior of the average IC-XT with respect to wavelength for the three WDM transmission schemes is evident.

Once we validated the correct implementation of the random perturbations, we proceed to repeat the simulations using the nonlinear coefficient $\gamma_p = 2.14\ \mathrm{W^{-1}\,km^{-1}}$. In this sense, we propagate again at core 1 the WDM scheme 1 centered at 1510 nm, with dispersion parameter $D = -3.4\ \mathrm{ps/nm \cdot km}$. The results after 500 m of nonlinear propagation are shown in Fig. 6 for two different input powers per WDM channel: 5 mW (6.989 dB) and 10 mW (10 dB), respectively.

According to Fig. 6, for a WDM transmission scenario in core 1 with negative dispersion, the central WDM channels decrease in power with respect to the outer channels due to FWM nonlinearity. In the same way, this power transfer from the central channels to the outer channels is more notorious if we employ a higher input power per WDM channel. On the other hand, while the WDM plan is propagated through core 1, we simultaneously simulate the signal that is coupled to core 2 and calculate the IC-XT according to the equation $XT = |A_2(z)|^2/|A_1(z)|^2$. It is important to remark that, during the simulation process, random bending and twisting perturbations are introduced along the fiber and these random perturbations affect directly the signal coupled to core 2. If we simulate only one propagation along the MCF, we obtain a typical random crosstalk at core 2 for each WDM channel, as is shown in Fig. 7(a). We denote this crosstalk as "single crosstalk." On the other hand, if we simulate 1000 runs, the random crosstalk at core 2 for each simulation will be different than what is shown in Fig. 7(a), but the "average crosstalk" will follow a deterministic curve in a function of wavelength as is shown in Fig. 7(b) for all WDM channels.

Now, if we compare the output of core 1 and core 2, we can observe that the power transfer among the transmitted WDM channels at core 1 shown in Fig. 6 is replicated in the average crosstalk at core 2 [Fig. 7(b)] with a slight tilt that corresponds to the linear wavelength dependence of the coupling coefficient (Fig. 5). This is not the case if we consider a single crosstalk [Fig. 7(a)]. These results indicate that the random bending and twisting introduced along the fiber modify in a random way the value of crosstalk for each WDM channel, but after averaging,

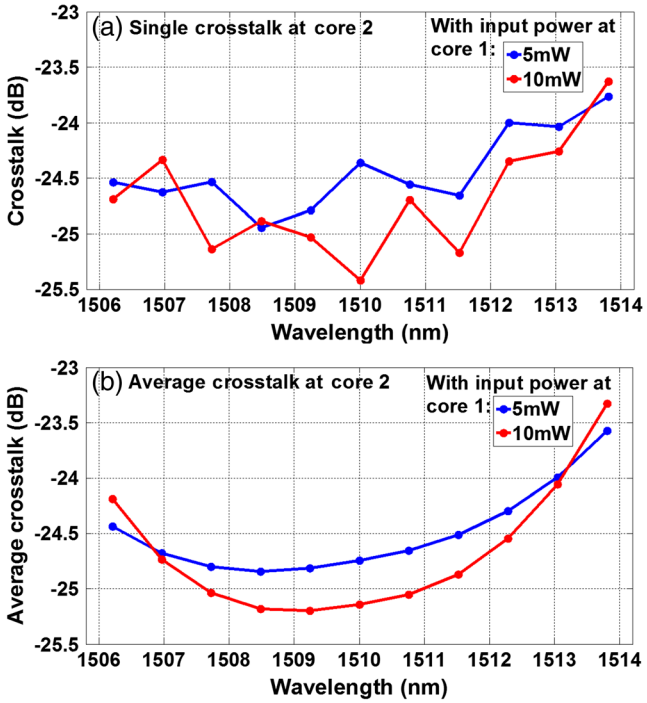

Fig. 7 Crosstalk of 11 WDM channels centered at 1510 nm in core 2 for a propagation length of 500 m using different input powers per WDM channel at core 1: 5 mW (blue curve) and 10 mW (red curve). (a) Single crosstalk and (b) average crosstalk.

the random effect on the coupling process is reduced and the average crosstalk at core 2 can reproduce the power profile of the WDM channels obtained at core 1.

We then repeated the numerical experiment considering the WDM transmission scheme 2 composed of 11 WDM channels centered at 1550 nm with dispersion parameter $D = 0$. The results after 500 m of nonlinear propagation through core 1 are shown in Fig. 8 for two different input powers per channel: 5 mW (6.989 dB) and 10 mW (10 dB), respectively.

According to Fig. 8, for a WDM transmission scenario with zero dispersion, we observe that the power transfer among WDM channels follows a different behavior if the channels are located at longer or shorter wavelengths with respect to the zero-dispersion wavelength. In the same way, this behavior is more notorious if we employ a higher input power per WDM channel at core 1. On the other hand, we calculate a single crosstalk and the average crosstalk for the WDM transmission scheme 2 centered at 1550 nm such as is shown in Fig. 9.

After a comparison of Figs. 8 and 9(b), we also can observe how the power profile of WDM channels obtained at core 1, which are caused by intracore nonlinearities, are replicated in the average crosstalk at core 2 with a slight tilt caused by the wavelength dependence of the coupling coefficient [Fig 9(b)]. It is important to note that this behavior is not observed again when considering a single random crosstalk [Fig. 9(a)].

Finally, we repeat the numerical experiment considering the WDM transmission scheme 3 composed of 11 WDM channels centered at 1590 nm with dispersion parameter $D = +3.4$ ps/nm $\cdot$ km. The results after 500 m of propagation through core 1 are shown in Fig. 10 for two different input powers per channel: 5 mW (6.989 dB) and 10 mW (10 dB), respectively.

According to Fig. 10, for a WDM transmission scenario with positive dispersion, we observe now that the central WDM channels increase in power with respect to the outer channels due to fiber nonlinearities, with this increment in power of the central channels being more notorious if we employ a higher input power per channel at core 1. On the other hand, the results shown in Fig. 11 correspond to a single random crosstalk and the average crosstalk of 11 WDM channels centered at 1590 nm. Similar to the above cases, we also can observe that the power profile of WDM channels obtained at core 1 are replicated in the average crosstalk at core 2 [Fig 11(b)]; however, this is not the case for a single random crosstalk [Fig. 11(a)].

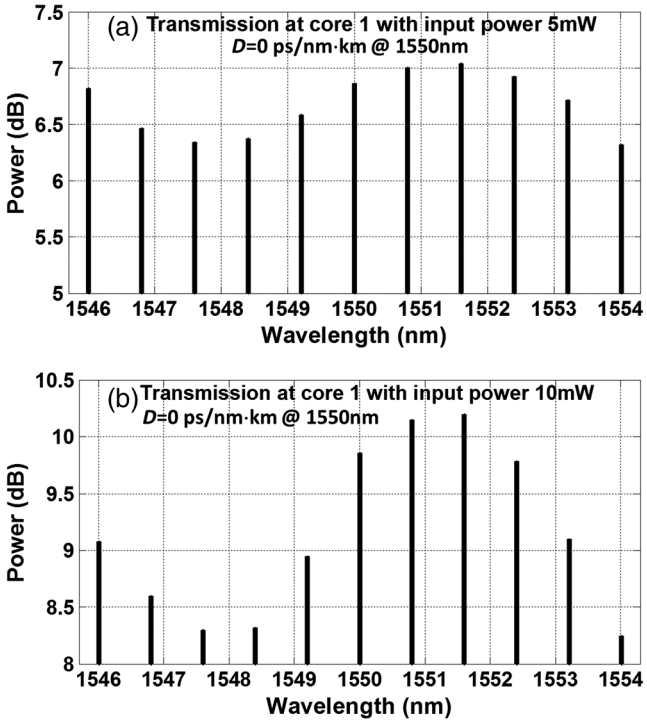

Fig. 8 Transmission of 11 WDM channels centered at 1550 nm in core 1 for a propagation length of 500 m with (a) 5 mW (6.99 dB) and (b) 10 mW (10 dB) of input power per WDM channel.

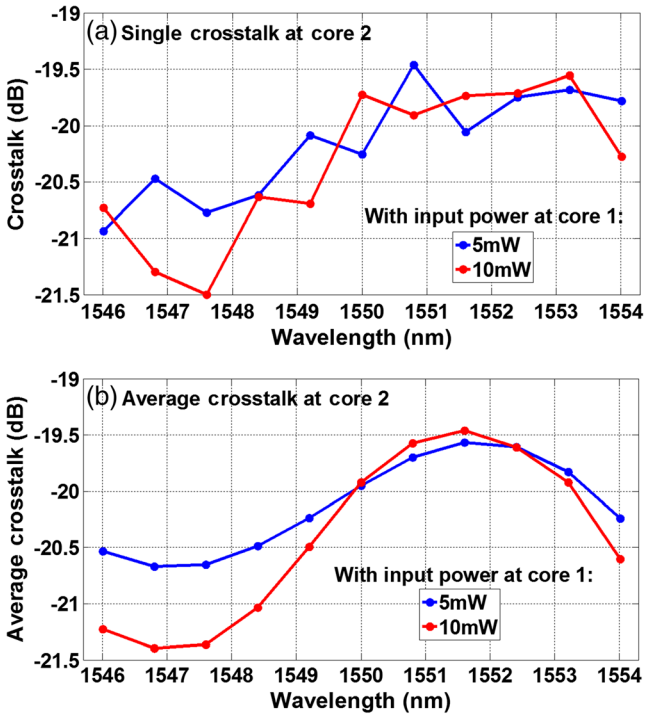

Fig. 9 Crosstalk of 11 WDM channels centered at 1550 nm in core 2 for a propagation length of 500 m using different input powers per WDM channel at core 1: 5 mW (blue curve) and 10 mW (red curve). (a) Single crosstalk and (b) average crosstalk.

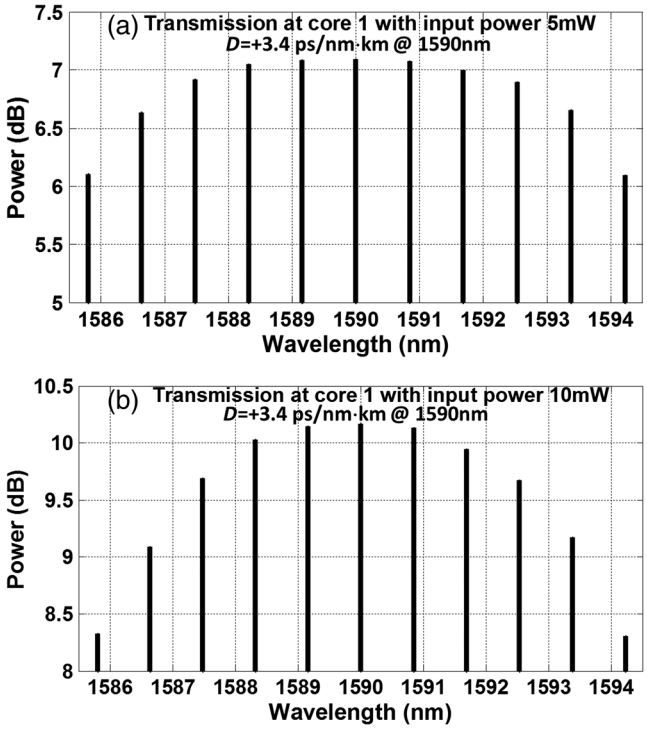

Fig. 10 Transmission of 11 WDM channels centered at 1590 nm in core 1 for a propagation length of 500 m with (a) 5 mW (6.99 dB) and (b) 10 mW (10 dB) of input power per WDM channel.

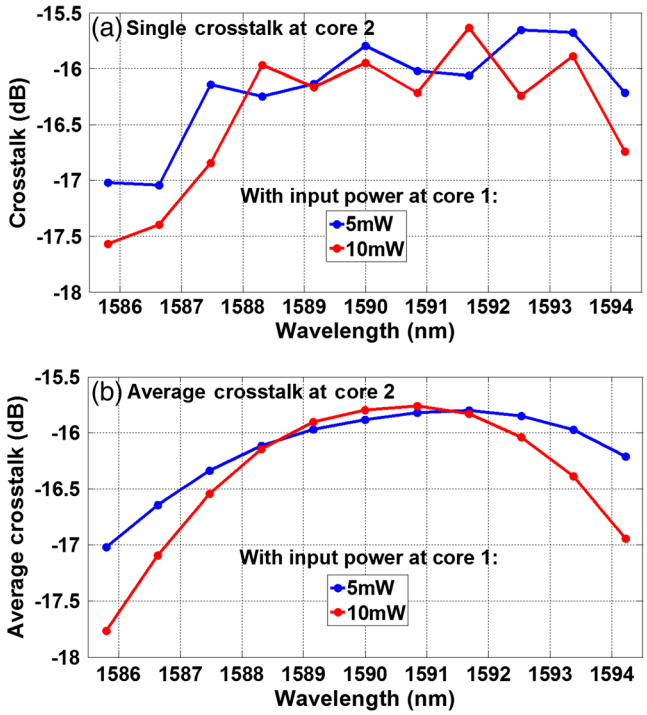

Fig. 11 Crosstalk of 11 WDM channels centered at 1590 nm in core 2 for a propagation length of 500 m using different input powers per WDM channel at core 1: 5 mW (blue curve) and 10 mW (red curve). (a) Single crosstalk and (b) average crosstalk.

In our analysis, we note that, for the three WDM transmission schemes, the average IC-XT at core 2 can then be modified by considering the power transfer among WDM channels produced at core 1 by intracore nonlinearities. In particular, the average IC-XT at core 2 follows a deterministic curve in a function of wavelength that can be predicted considering the superposition of the power profile among WDM channels obtained at the output of core 1, which is caused by intracore nonlinearities, and the linear wavelength dependence of the average IC-XT described in Fig. 5. In addition, a positive, zero, or negative dispersion parameter modifies the nonlinear effects among WDM channels in different way at core 1. Then, by choosing a specific dispersion parameter in the fiber cores of a homogeneous MCF in combination with nonlinear effects among the WDM channels, we could at first instance modify the wavelength dependence of the average crosstalk of WDM channels along the fiber. It is worth mentioning that this affirmation only applies if we consider an average crosstalk at core 2 for multiple WDM channels propagated in a MCF under random bending and twisting perturbations. Furthermore, if we only consider a single random crosstalk instead of an average crosstalk, the wavelength dependence of the crosstalk is not predictable and does not follow a deterministic behavior. This is due to the coupled signal at core 2 denoted by $A_2(z)$ only depending on two parameters: the linear coupling coefficient q_{12} and the phase mismatch between cores $\Delta\phi_{1,2}(z)$. The phase mismatch $\Delta\phi_{1,2}(z)$ will be different for all WDM channels because it depends on wavelength [see Eq. (6)]. In addition, $\Delta\phi_{1,2}(z)$ is modified along the fiber due to random bending and twisting perturbations; as a consequence, we obtain a single random crosstalk with an aleatory behavior in a function of wavelength for all WDM channels.

On the other hand, the power transfer among WDM channels caused by intracore nonlinearities at core 1 can also be manipulated, not only by the value of the dispersion parameter of the fiber core but also by modifying the characteristics of the WDM plan transmitted along the MCF, such as the input power per WDM channel, the number of WDM channels, and the interchannel spacing. In our analysis, only variations of the input power per channel were considered from 5 to 10 mW, obtaining an increment of the power transfer among WDM channels for higher input powers. This nonlinear effect is attributed to FWM nonlinearity. The power transfer among WDM channels produces channels with different powers at the output of core 1 with power differences ranging from 1 to 1.5 dB in cores with negative (Fig. 6) or positive (Fig. 10) dispersion parameters and power differences among WDM channels from 0.5 to 2 dB in cores with zero dispersion parameter (Fig. 8). These power differences among WDM channels are transferred by linear coupling to the average crosstalk at the output of core 2, but not for a single random crosstalk, as was mentioned above. These results indicate that, after an averaging process, the random effect of bending and twisting perturbations along the fiber is reduced and the average crosstalk at core 2 can reproduce the power differences observed among the WDM channels obtained at core 1 by intracore nonlinearities. These results provide valuable information for understanding the wavelength dependence of the average IC-XT of WDM channels in MCF systems working around a zero-dispersion wavelength. It is interesting to emphasize how the sign of the dispersion parameter affects the way the power is redistributed among WDM channels in core 1 caused by FWM. In the anomalous dispersion regime ($D > 0$ or $\beta_2 < 0$), the power tends to concentrate in the central channels, whereas the opposite occurs when dispersion is normal ($D < 0$ or $\beta_2 > 0$); these differences can be observed in Figs. 6 and 10. Note that this difference between anomalous and normal dispersion was already identified in Ref. 17 using fibers with only a single core. At first instance, this difference could be attributed to the phase mismatch generated among WDM channels during propagation in core 1. According to Ref. 13, in a degenerate case of FWM, the phase mismatch is given by $\Delta\beta = \beta_2\Omega^2$, where Ω represents the channel spacing. The sign of the phase mismatch is given by the GVD parameter β_2, and it might affect the power transfer among WDM channels in the normal and anomalous regimen in core 1. Consequently, the average IC-XT of WDM channels produced in core 2 under a weak coupling regimen, where only linear coupling coefficients are considered, can show a similar behavior to that observed in core 1 in the normal and anomalous regimen. These observations contribute new information with respect to the results obtained in Refs. 7 and 8, where only MCFs with positive dispersion parameters were employed.

Finally, the average IC-XT of WDM channels is an important issue in MCF communication systems. In particular, our results provide useful insights into the behavior of this average IC-XT

at different wavelengths in cases in which MCFs with negative, zero, or positive dispersion parameters are employed in communication systems. With this information, we could select the most convenient modulation formats and FECs for different groups of WDM channels that propagate in each core to improve the performance. In addition, if we consider dispersion management systems based on multiple MCF sections with positive and negative dispersion parameters, it could be possible to uniformize the average IC-XT of WDM channels due to the opposite effect observed in Figs. 7(b) and 11(b), which is useful at the end of the communication system; however, further analysis must be performed in this context.

4 Conclusions

The dispersion impact on the average crosstalk among WDM optical channels transmitted in a two-core fiber system was numerically analyzed for three-channel plans centered at different positions relative to the zero-dispersion wavelength. We have found that the dispersion parameter D significantly affects the average IC-XT of WDM optical channels. In particular, the average IC-XT of multiple WDM channels follows a deterministic curve in a function of wavelength that can be predicted considering the superposition of the power profile among WDM channels obtained at output of core 1, which is caused by intracore nonlinearities and the linear wavelength dependence of the average IC-XT. In addition, the effect of the FWM nonlinearity on the power level of the transmitted WDM channels at core 1 depends on D, and this effect is transferred by a linear coupling process to the average crosstalk of WDM channels at core 2. Then, the average IC-XT of WDM channels can be modified in a controlled way by selecting an adequate dispersion parameter D in combination with four-wave mixing nonlinearity. These results provide valuable information for understanding the wavelength dependence of the average IC-XT of homogeneous multichannel MCF systems working around a zero-dispersion wavelength.

Acknowledgements

The authors are grateful to Engineering Institute at UNAM in Mexico and the Optical Sciences group at the University of Twente in the Netherlands.

References

1. T. Hayashi et al., "Design and fabrication of ultra-low crosstalk and low-loss multi-core fiber," *Opt. Exp.* **19**(17), 16576–16572 (2011).
2. T. Hayashi et al., "Physical interpretation of intercore crosstalk in multicore fiber: effects of macrobend, structure fluctuation, and microbend," *Opt. Exp.* **21**(5), 5401–5412 (2013).
3. S. Mumtaz, R. J. Essiambre, and G. P. Agrawal, "Reduction of nonlinear penalties due to linear coupling in multicore optical fibers," *IEEE Photonics Technol. Lett.* **24**(18), 1574–1576 (2012).
4. Q. Yao et al., "Crosstalk aware routing, spectrum, and core assignment in space-division multiplexing optical networks with multicore fibers," *Opt. Eng.* **56**(6), 066104 (2017).
5. F. Ye et al., "Wavelength dependence of inter-core crosstalk in homogeneous multi-core fibers," *IEEE Photonics Technol. Lett.* **28**(1), 27–30 (2016).
6. R. S. Luís et al., "Investigation of inter-core crosstalk and Raman nonlinearity in wideband MCF transmission," in *Proc. Opt. Fiber Comm. Conf.*, p. Th4H.6 (2017).
7. D. Ceballos-Herrera, R. Gutierrez-Castrejon, and J. Alvarez-Chavez, "Stimulated Raman scattering and four wave mixing effects on crosstalk of multicore fibers," *IEEE Photonics Technol. Lett.* **30**(1), 63–66 (2018).
8. D. Ceballos-Herrera, M. Lopez-Coyote, and R. Gutierrez-Castrejon, "Crosstalk characteristics of WDM channels in quasi-homogeneous multicore fibers," *IEEE Photonics Technol. Lett.* **32**(13), 759–762 (2020).
9. A. V. T. Cartaxo and T. M. F. Alves, "Discrete changes model of inter-core crosstalk of real homogeneous multi-core fibers," *J. Lightwave Technol.* **35**(12), 2398–2408 (2017).

10. A. Cartaxo et al., "Dispersion impact on the crosstalk amplitude response of homogeneous multi-core fibers," *IEEE Photonics Technol. Lett.* **28**(17), 1858–1861 (2016).
11. D. Kumar and R. Ranjan, "Design and cross talk optimization in single-mode high-core count multicore fiber under limited cladding diameter," *Opt. Eng.* **58**(5), 056109 (2019).
12. D. Kumar and R. Ranjan, "Optimal design of a single-mode trench-assisted homogeneous multicore fibre with a minimum crosstalk level," *Quantum Electron.* **49**(11), 1045–1053 (2019).
13. G. P. Agrawal, *Nonlinear Fiber Optics*, 3rd ed., Academic Press, San Diego, California (2001)
14. D. Hollenbeck and C. Cantrell, "Multiple-vibrational-mode model for fiber-optic Raman gain spectrum and response function," *J. Opt. Soc. Am. B.* **19**(12), 2886–2892 (2012).
15. J. W. Fleming, "Dispersion in GeO_2-SiO_2 glasses," *App. Opt.* **23**(24), 4486–4493 (1984).
16. A. Ortega-Monux et al., "Enhanced accuracy in fast-Fourier-based methods for full-vector modal analysis of dielectric waveguides," *IEEE Photonics Technol. Lett.* **18**(10), 1128–1130 (2006).
17. F. Vanholsbeeck et al., "Coupled-mode analysis of stimulated Raman scattering and four-wave mixing in wavelength-division multiplexed systems," *Opt. Commun.* **250**(1), 191–201 (2005).

Biographies of the authors are not available.